

STRUCTURAL AND ELECTROCHEMICAL PROPERTIES OF P3-Na_{0.67}Mn_{0.3}Co_{0.7}O₂ NANOSTRUCTURES PREPARED BY CITRIC-UREA SELF-COMBUSTION ROUTE AS CATHODE FOR SODIUM ION BATTERY

M. Z. ABDULLAH^{a,b}, M. H. AL-TIMIMI^{a,c}, W. H. ALBANDA^{a,d},
M. DUMITRU^e, A. E. BALAN^a, C. CEAUS^a, E. TANASA^f, I. STAMATIN^{a*}

^aUniversity of Bucharest, Faculty of Physics, 3Nano-SAE Research Centre, 405 Atomistilor str., PO Box MG-38, Bucharest-Măgurele, Romania

^bMaterials Research Directorate, Ministry of science and technology, Iraq

^cPhysics Department, College of Science, University of Diyala, Iraq

^dScience Department - College of basic Education, Mustansiriyah University, Iraq

^eNational Institute for Laser, Plasma & Radiation Physics (INFLPR), Romania

^fPolitehnica University of Bucharest, 313 Splaiul Independentei, Bucharest, Romania

Sodium ion battery is a promising alternative for lithium ion battery due to the abundance of raw materials and effective-cost advantages. This paper reports on a distinguished sodium insertion host material, pure ideal layered P3-type Na_{0.67}Mn_{0.3}Co_{0.7}O₂ nanostructure (Rhombohedral space group R3m no.160) synthesized the first time using novel citric-urea self-combustion route in air. Different calcination temperatures were corroborated with morphology, crystalline structure and electrochemistry performance as cathodes for sodium ion battery. Increasing the calcination temperature has significant effect on the structural and electrochemical properties; ideal layered P3-type Na_{0.67}Mn_{0.3}Co_{0.7}O₂ cathode calcined at 800°C has the highest specific discharge capacity of 158.3 mAh/g at 0.25C with capacity retention about (99.6%). The improvement of electrochemical performance results from the high crystalline growth of P3-type Na_{0.67}Mn_{0.3}Co_{0.7}O₂ cathode as a function of calcination temperature increasing. The electrochemical performance represents a step further for the achievement of sustainable sodium ion battery as electric energy storage.

(Received July 12, 2019; Accepted December 16, 2019)

Keywords: Energy storage, Battery, Layered structures

1. Introduction

Recently, the demand of lithium grew in technology as its wide range of applications such as electric vehicles, phones and laptops etc. so, it is important to find an alternative to a lithium battery. On earth, the lithium resources are very rare and costly compared with sodium, the presence of lithium is evaluated at 0.006 wt.% while for sodium to 2.64 wt%, and also sodium metal is available in different forms as sea salt, rock salt and quite regularly distributed in the whole world with advantages; easy access and extraction, in addition, the electrochemical properties of sodium are similar to lithium, because they are situated at the same group in elements periodic table. Sodium ion battery technology became a promising candidate to develop battery systems with low cost for replacing lithium ion battery in several applications [1, 2]. The sodium ion battery is much cheaper and lighter than lithium considering the total cost of the battery, the replacement of expensive and heavy copper anodic current collector used in lithium battery (lithium doesn't alloy with copper but it alloys with aluminum while Na doesn't alloy with aluminum) with lightweight and cheap aluminum anodic current collector is an important feature

* Corresponding author: istarom@3nanosae.org

that leads to lighter sodium ion battery compared to lithium with lower cost and increased energy density, due to lower ion size of aluminum anodic collectors, which is considered advantageous [3].

The research and investigations on sodium ion batteries have increased significantly in recent years with good progress, but the electrochemical performance of sodium battery has not yet reached the ambition level compared to lithium battery. The researchers have shifted their attention to sodium based multilayer transition metal cathodes Na_xMO_2 (M such as Co, Ni, Mn etc.) depending on the knowledge derived from lithium battery development, which can be divided into two main groups; O-type structures (octahedral sites) and P-type structures (prismatic sites), determined by the nature of alkali ions sites between the transition metal oxide layers [4, 5, 6], the Na based layered transition metal oxides cathodes can be also arranged in various structure types within these two groups such as O3, P3 and P2 which mainly depends on several parameters as stoichiometric proportions of sodium in the cathode composition, calcination temperature and preparation method, these parameters plays an important role to the layered structure type [7]. M. Sathiya et al. synthesized pure O3-type $\text{NaNi}_{0.33}\text{Mn}_{0.33}\text{Co}_{0.33}\text{O}_2$ as cathode for Na ion battery by sol-gel method with delivered capacity of about 120 mAh/g and study the phase stability by X-ray diffraction [8]. Present studies have indicated that layered P-type structures are considered promising candidates as cathodes for Na ion battery due to their distinctive electrochemical performances. X. Wang et al. provided detailed discussion about the electrochemical and structural properties of P2- $\text{Na}_{2/3}\text{Mn}_y\text{Co}_{1-y}\text{O}_2$ synthesized by one step solid state method, presenting delivered discharge capacity 123 mAh/g at the first discharge cycle which decreased gradually with battery cycling [9].

Generally, finding the effective combination of cathode materials by developing the preparation methods with different parameters to control the cathode structures and crystallization degrees the shortest way to improve the electrochemical performance of sodium battery. In this contribution, layered P3-type NaMnCoO_2 cathodes were successfully synthesized the first time by novel citric-urea self-combustion route, the effect of calcination temperature on the structural and electrochemical properties were discussed in detail. Increasing the calcination temperature led to an improvement of crystallization degree for Na ion battery cathodes and stabilizes the P3-type structure. Distinctive electrochemical performance was achieved with delivered discharge capacity 158.3 mAh/g at 0.25C and good rate capability. This study indicates that the ideal layered P3-type $\text{Na}_{0.67}\text{Mn}_{0.3}\text{Co}_{0.7}\text{O}_2$ calcined at 800°C can be efficient candidate cathode for the sake of future development of sodium ion battery.

2. Experimental

Sodium nitrate NaNO_3 , $M_w=84.9947$ g/mol; Manganese acetate tetrahydrate $\text{Mn}(\text{CH}_3\text{COO})_2 \cdot 4\text{H}_2\text{O}$, $M_w=245.086$ g/mol, Cobalt acetate tetrahydrate, $\text{Co}(\text{CH}_3\text{COO})_2 \cdot 4\text{H}_2\text{O}$, $M_w=249.09$ g/mol; citric acid, $\text{C}_6\text{H}_8\text{O}_7$, $M_w=192.124$ g/mol; urea $\text{CO}(\text{NH}_2)_2$, $M_w=60.06$ g/mol and nitric acid HNO_3 (70%), $M_w=63.01$ g/mol. All reagents are analytical grade and purchased from different suppliers. They are used without further purification.

The pure NaMnCoO_2 cathode powders were prepared by citric-urea self-combustion route, A stoichiometric amounts of sodium nitrate NaNO_3 (2.12 g, 25 mM) as precursor of Na ions, manganese acetate $\text{Mn}(\text{CH}_3\text{COO})_2 \cdot 4\text{H}_2\text{O}$ (12.25g, 50 mM) and cobalt acetate $\text{Co}(\text{CH}_3\text{COO})_2 \cdot 4\text{H}_2\text{O}$ (12.45 g, 50 mM) were completely dissolved in distilled water and then mixed together with continuously stirring respectively, aqueous solution of citric acid $\text{C}_6\text{H}_8\text{O}_7$ (28.8 g, 150 mM) and urea $\text{CO}(\text{NH}_2)_2$ (4.5 g, 75 mM) were added to the first solution with continuous mixing to obtain the starting solution (100 ml), the molar ratio of citric acid (1:2) and urea (1:1) of total metal ions. Finally, concentrated nitric acid HNO_3 was added to the starting solution in the volume ratio (1:0.1) with continuous stirring. The starting solution heated at 120°C to remove the water. After 4 hours the formation of dark purple resin with alternating foaming was observed until dark purple gel was obtained. The gel was dried in oven at 180°C overnight (12 hours), the volume for the gel was significantly expanded, about 20 times, comparing with the initial volume, to form high porous NaMnCoO_2 polymeric intermediate, and then the NaMnCoO_2 polymeric intermediate was

calcined at different temperature 400, 600 and 800°C in air for four hours, as shown in Figure. 1 (a, b, c, d).

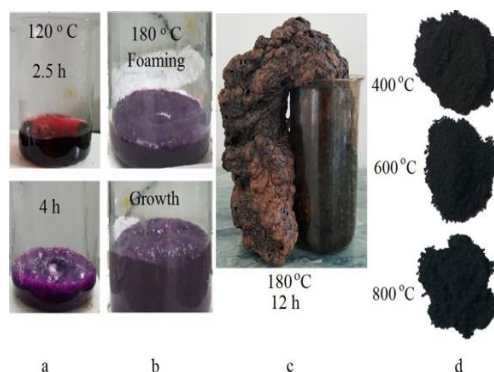


Fig. 1. Preparation protocol.

3. Results and discussions

3.1. Topographic study

The surface morphology of obtained sodium manganese/cobalt oxide powders was analyzed using a scanning electron microscope InspectS (FEI) with accelerating voltage of 20 kV. Figure.2 (a, b, c, d) presents the morphology of polymeric intermediate before and after the calcination process at different temperatures (400,600 and 800°C) to investigate the calcination temperature effect on the structural evolution. The morphology images for polymeric intermediate before calcination as shown in Figure.2 (a) obviously confirmed a high porous amorphous structure consisting of different amorphous phases assigned to sodium, manganese and cobalt metallic amorphous citrates, the high porosity occurs due to the release of CO₂, NH₃ and NO₂ gases during the drying process at 180°C as well as attributed to the presence of citric acid which improves the polymerization process [10,11].

On the other hand, from SEM image for polymeric intermediate one can notice clearly that there are very small white beads crystals on the surface, this confirming the XRD results which indicate the formation of tetragonal phase for the powder before calcination process, these crystal beads can be seeds for crystal growth.

SEM images of the powders after the calcination process at 400, 600 and 800°C, presented by Figure. 2 (b, c, d), reveals that the powder calcined at 400°C starts the crystallization process, transforming from the amorphous gel to the crystalline Na_{0.67}Mn_{0.3}Co_{0.7}O₂, corresponding with the X-ray diffraction that show the formation of rhombohedral phase, the crystallization degree increasing with the rise of the calcination temperature. The crystallization process was fully completed at 800°C, resulting the high porosity crystalline Na_{0.67}Mn_{0.3}Co_{0.7}O₂ powder with high purity with desired cations ratios for required composition at molecular level) which is the most important features of the sol-gel combustion method [11]. The full crystalline growth and high porosity of the resulting powder indicates the proper adjustment of sodium nitrate ratio to complexants (citric acid and urea) and proper flaming time, in this way the particle aggregation was avoided and the porosity was increased [12]. The flaming phenomenon was observed during the calcination process as the increase in the powder volume as double the initial volume. Figure.3 shows crystallite particle-like at 800°C.

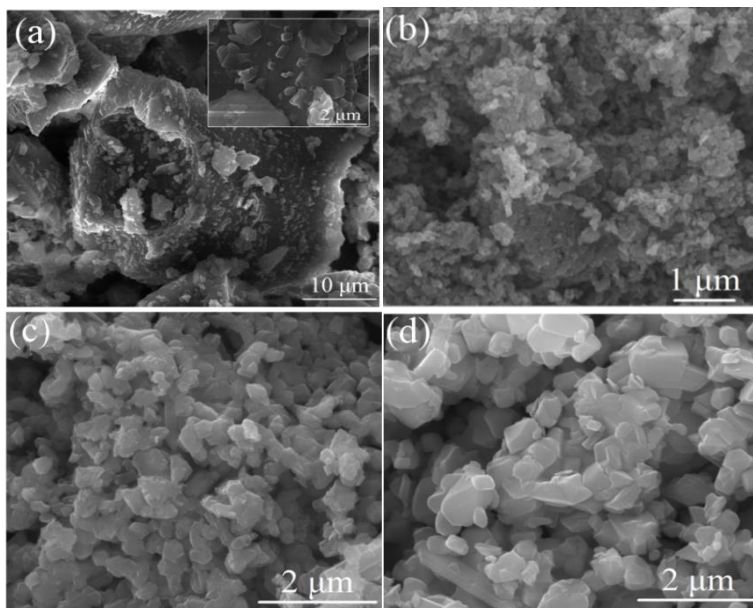


Fig. 2. SEM images of porous NaMnCoO₂ polymeric intermediate (a) before calcination; (b) 400°C; (c) 600°C (d) 800°C.

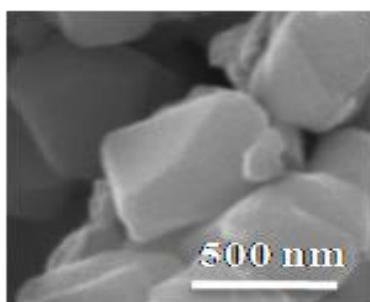


Fig. 3. Crystallite particle-like form at 800°C.

3.2. Crystallographic study

To determine the crystalline structure of the synthesized powders, X-ray diffraction patterns of polymeric intermediate and calcined powders at different temperatures (400, 600 and 800°C) depicted in Fig. 4 (a), were acquired using (XRD-6000 powder, Shimadzu) diffractometer with Cu K_α radiation, in the 2θ range 10° to 70° with scan rate of 2° min⁻¹.

Fig. 4 (a), presents the X-ray pattern for polymeric intermediate before calcination, exhibiting amorphous phase with very small peaks at (2θ=29.37 °) (112) d-space 3.045 Å and (2θ = 38.99 °) (004) d-space 2.308 Å, which can indicate the creation of tetragonal phase within the amorphous phase according to space group I41/amd no. 141 [13] after drying process of the prepared resin at 180 °C overnight.

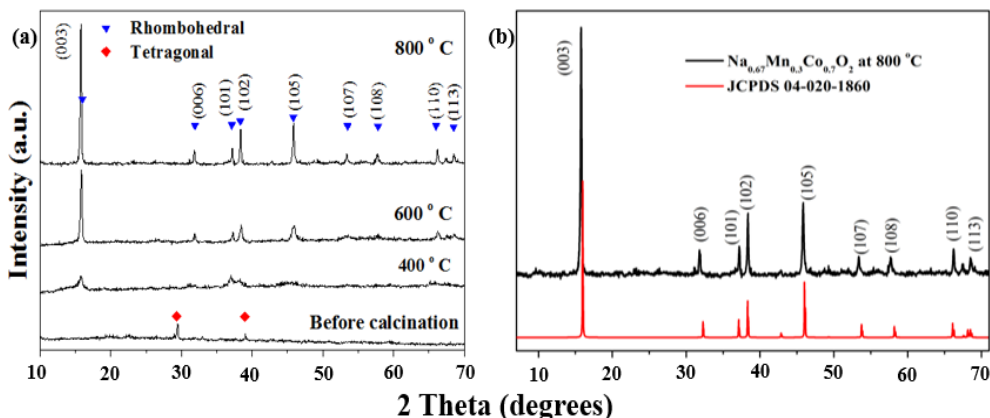


Fig. 4. (a) X-ray diffraction patterns for NaMnCoO_2 polymeric intermediate and calcined powders at different temperatures (400, 600 and 800 °C); (b) Comparison with JCPDS 04-020-1860 (Rhombohedral R3m no.160 [14,15]).

The X-Ray diffraction patterns for calcined powders at 400, 600 and 800 °C, presented in Fig. 4 (a), demonstrates that the layered NaMnCoO_2 nanostructure peaks began to form at calcination temperature 400 °C, the peaks grow sharper with the increase of calcination temperature to 600 °C and then the final ideal layered P3-type $\text{Na}_{0.67}\text{Mn}_{0.3}\text{Co}_{0.7}\text{O}_2$ rhombohedral nanostructure was obtained at 800 °C, comparing with Rhombohedral R3m no.160 [14,15,16]. The crystalline growth during the calcinations process of the prepared powders resulted due to the tendency of reducing the interfacial surface energy [17]. On the other hand, the XRD patterns of powders calcinated at high temperatures 600 and 800 °C reveals the structural stability of obtained $\text{Na}_{0.67}\text{Mn}_{0.3}\text{Co}_{0.7}\text{O}_2$ during calcinations process. The X-ray diffraction reveals the relation between the calcination temperature and crystal growth, rising the calcinations temperature leads to the increase of the crystal growth obtaining the final crystalline structure at 800 °C, agreeing with SEM and TG results.

The XRD pattern for the final product at 800 °C, Figure 4.(b), presents three strong main peaks at ($2\theta = 15.9^\circ$) (003) d-space 5.54 Å, ($2\theta = 38.4^\circ$) (102) d-space 2.34 Å and ($2\theta = 45.8^\circ$) (105) d-space 1.97 Å and other several peaks at ($2\theta = 31.7^\circ$) (006) d-space 2.77 Å, ($2\theta = 37.2^\circ$) (101) d-space 2.42 Å, ($2\theta = 53.5^\circ$) (107) d-space 1.7 Å, ($2\theta = 57.8^\circ$) (108) d-space 1.58 Å, ($2\theta = 66.09^\circ$) (110) d-space 1.41 Å and ($2\theta = 68.49^\circ$) (113) d-space 1.36 Å, corresponding with Rhombohedral P3-type structure[16](JCPDS 04-020-1860) proving the formation of pure $\text{Na}_{0.67}\text{Mn}_{0.3}\text{Co}_{0.7}\text{O}_2$. From the XRD patterns of powders calcined at 400, 600 and 800 °C one can observe that there are no peaks attributed to impurities, this is proof that all the reacting metals ions in this preparation method entered the transition metal layers to obtain NaMnCoO_2 powders with ideal Orthorhombic P3-structure type.

3.3. Energy dispersion X-ray spectroscopy (EDS)

EDS technique was used to evaluate the chemical composition for the prepared powders, using a FEI InspectS microscope equipped with an ELEMENT EDAX analyzer, using acceleration voltage of 20 kV. The EDS results are presented in Figure.5 and Table 1, the emission peaks for polymeric intermediate and calcined powders at 400, 600 and 800 °C, and the quantification for all the samples were investigated for each powder as presented in Table 1.

The EDS spectra reveals that only sodium, manganese, cobalt and oxygen elements were detected after the calcination process as well as nitrogen and carbon for polymeric intermediate powder before calcination. It is important to note that the EDS quantification cannot be considered rigorous, due to the fact that these analyses were carried out in standardless mode, the quantification is rather qualitative but very useful for evaluating the chemical evolution during calcination. Table 1. shows that during calcination, nitrogen and carbon are depleted while the

oxygen level decreases due to the release of CO₂ and NO₂, this is also proved by Thermogravimetric Analysis.

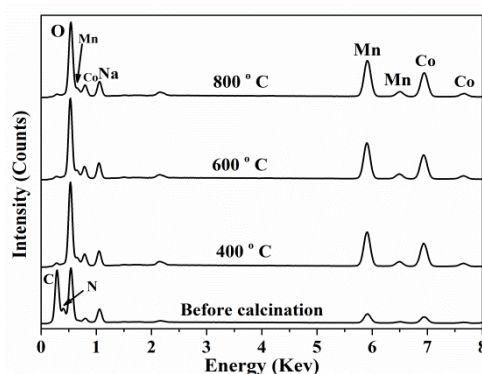


Fig. 5. EDS spectra for NaMnCoO₂ polymeric intermediate and calcined powders at 400, 600 and 800°C.

Table 1. EDS quantification of NaMnCoO₂ polymeric intermediate before calcination and calcined 400, 600 and 800°C.

Elements ratios of NaMnCoO ₂ before calcination			
Element	Weight (%)	Atomic (%)	Error (%)
C	21.34	29.1	7.11
N	19.52	22.83	9.06
O	38.08	38.99	9.09
Na	7.13	5.08	8.33
Mn	6.74	2.01	2.65
Co	7.18	2	2.4
Elements ratios of NaMnCoO ₂ calcined at 400 °C			
O	21.36	42.81	5.58
Na	15.44	21.54	9.43
Mn	30.39	17.73	2.06
Co	32.75	17.81	2.15
Elements ratios of NaMnCoO ₂ calcined at 600 °C			
O	20.13	41.11	5.61
Na	15.4	21.88	9.45
Mn	31.23	18.57	2.04
Co	33.24	18.43	2.16
Elements ratios of NaMnCoO ₂ calcined at 800 °C			
O	18.09	37.99	5.69
Na	15.67	22.9	9.46
Mn	32.27	19.74	2.02
Co	33.97	19.37	2.18

These results revealed that inorganic stable structures were obtained by polymeric citrate-urea route after calcination process at 400, 600 and 800°C in the same layered P3-type nanostructure which agrees well with XRD and TG results. The XRD and EDS results agrees that there is no evidence of any impurities in obtained layered NaMnCoO₂ powders after the calcination process.

3.4. Thermogravimetric analysis (TGA)

TGA was used to determine the optimum calcination temperature for the desired morphology and crystallography. The thermal analysis for NaMnCoO₂ polymeric intermediate was

performed with thermo gravimetric (Mettler Toledo- Star System) analyzer to define the thermal behavior and phase transitions of prepared sample, the test was achieved with a heating rate of $12^{\circ}\text{C min}^{-1}$ in static air until 1000°C , and then the TGA / DTGA curves were obtained. Figure.6 presents the thermal behavior profile of NaMnCoO_2 polymeric intermediate as source for layered P3-type NaMnCoO_2 nanostructures.

The (TGA/DTGA) curves revealed that there are three weight loss regions, the first region shows that the sample lost approximately (5 wt.%) of the initial weight until the temperature 85°C which can be assigned to removal of absorbed moisture from the atmosphere because of the high porous structure of polymeric intermediate. Between ($120 - 170^{\circ}\text{C}$) the sample lost approximately (2 wt.%) resulted from releasing the structural water of polymeric intermediate [18, 19], this stage is considered as dehydration process for the polymer intermediate in two different kinetics. The majority of weight loss was up to 200°C in the second and third regions, which were represented by the two strong exothermic transformation peaks at 268 and 368°C , in the temperature ranges $200 - 290^{\circ}\text{C}$ and $300 - 390^{\circ}\text{C}$ with major weight loss approximately (30 wt. %) and (35 wt. %) respectively, which can be attributed to the organic derivatives decomposition of polymeric intermediate as well as ignition phenomenon monitored at the temperature range $275 - 375^{\circ}\text{C}$, the presence of urea plays as an oxidizing agent that reduces the ignition temperature and combustion duration [20,21,22].

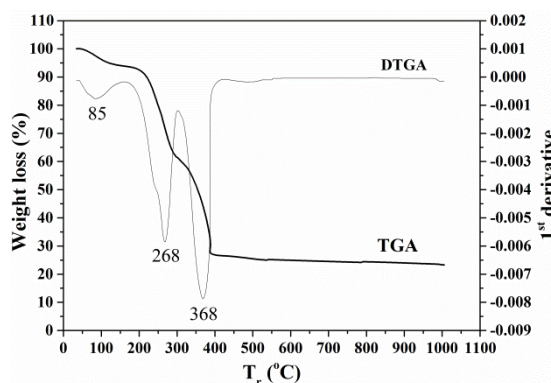


Fig. 6. TGA/DTG curves for NaMnCoO_2 polymeric intermediate before calcination.

From (TGA/DTGA) curves we observed that at 400°C , the NaMnCoO_2 polymeric intermediate almost decomposed completely to layered metal oxide, the weight loss of the sample stabilizes at 400°C , referring that the layered metal oxide had established at minimum calcinations temperature 400°C . The obtained structure is Rhombohedral; the crystalline growth is continuous in the same P3-type structure with increasing the calcination temperature to 600°C and the final product was completed at 800°C , this compares with SEM, XRD and EDX results. The TGA/DTGA curves became relatively straight after 400°C with weight loss approximately (3 wt. %) and can be assigned to evaporation the sodium (volatile sodium) [16,23]. In this work, the calcination temperatures (400 , 600 and 800°C) was suggested in order to get different morphologies for layered P3-type NaMnCoO_2 nanostructures and their effect on the electrochemical properties.

3.5. Fourier- transforms infrared spectroscopy (FTIR)

Fourier-transforms infrared spectroscopy (FTIR) was performed using (JASCO FT/IR-6200) spectroscope to investigate polymeric intermediate powder and calcined powders at different calcination temperature (400 , 600 and 800°C) in the characteristic range for NaMnCoO_2 ($400 - 800 \text{ cm}^{-1}$).

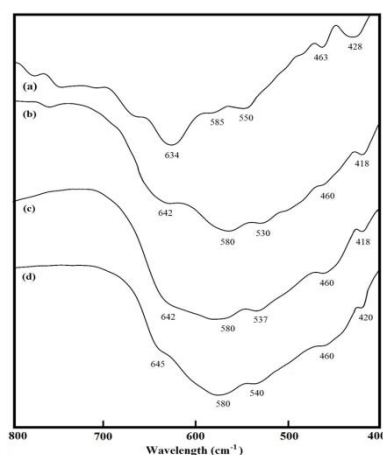


Fig. 7. FTIR spectra (a) *NaMnCoO₂* precursor before calcinations; (b) 400°C; (c) 600°C (d) 800°C.

The obtained FTIR spectra of prepared powders are presents in Fig. 7 (a, b, c, d) respectively, the wavelengths numbers of chemical bonds shown in Table 2. The IR spectrum of *NaMnCoO₂* polymeric intermediate exquisites five main bands in the range 400 – 800 cm^{-1} , sharp bands around 428 and 463 cm^{-1} , broad bands around 585 and 634 cm^{-1} attributed to bending and stretching vibrations of metal oxide layers MO_6 (M = Mn, Co) octahedral [24,25,26], and broad band around 550 cm^{-1} assigned to sodium oxide band (Na – O) [27].

After calcination process at (400, 600, 800°C), the bands became more defined, wide and shifted around the original positions with increasing the temperature, at calcination temperature 800°C, the bands 428, 463, 500 and 585 cm^{-1} shifted to low wavelength number at 420, 460, 540 and 580 cm^{-1} , the band 634 cm^{-1} shifted to high wavelength number and became broad band centered at 645 cm^{-1} , resulted from rearrangement the molecules in specific framework indicating to layered *NaMnCoO₂* structures were formed well corresponded with SEM, XRD and TGA results.

On the other hand, the obtained broad bands after calcination process as shown in FTIR spectra are distinctive from layered structure from spinel structure which has two symmetric band centered around 521 cm^{-1} and 617 cm^{-1} reflecting the high local symmetry of the cubic structure [28].

Table 2. Wavelength numbers for chemical bonds for *NaMnCoO₂* polymeric intermediate before calcination and calcined at 400, 600 and 800°C.

Samples	Peak 1 (cm^{-1})	Peak 2 (cm^{-1})	Peak 3 (cm^{-1})	Peak 4 (cm^{-1})	Peak 5 (cm^{-1})
Polymeric intermediate	428	463	550	585	634
400°C	418	460	530	580	642
600°C	418	460	537	580	642
800°C	420	460	540	580	645

3.6. Raman spectroscopy

Raman spectra of synthesized powders were registered by using (JASCO NRS-3100 laser Raman spectroscopy) in the characteristic range (100 – 700 cm^{-1}) with laser power (5 mW). Raman spectroscopy carried out to obtain information about the structural fingerprint of prepared powders by observing the vibration modes (rotational or vibrational), as supplementary

information along with the information collected from XRD and FTIR tests to completely characterize the powders structures. Fig. 8 (a, b, c, d) presents the Raman spectra for polymeric intermediate before calcination and calcined powders at (400, 600, 800°C) respectively. The obtained spectrum for polymeric intermediate showed that there are five main Raman active peaks around 166, 290, 481 cm^{-1} and wide band with two peaks at 556 and 632 cm^{-1} , after calcination process these peaks became more defined and shifted around their initial positions with increasing the calcination temperatures, to be clear peaks around 165, 279, 466, 560 and 611 cm^{-1} for calcined powder at 800°C which referred to formation of layered sodium – metal transition oxide [29, 30], the Raman peak numbers for all synthesized powders shown in Table 3. The peaks around 466 and 560 cm^{-1} attributed to the deformation and symmetric stretch of metal – oxygen (M = Na, Mn, Co – O) bonds in layered Na – metal transition oxide [31], and the peaks around 165 and 611 cm^{-1} are assigned to the oxygen bond vibrations within the neighboring layers in parallel to C – axis [30,32], the peak around 279 cm^{-1} can be assigned to manganese – oxygen band vibration within the layered metal transition, these well-defined Raman peaks at 800°C reveals a good crystallinity of layered $\text{Na}_{0.67}\text{Mn}_{0.3}\text{Co}_{0.7}\text{O}_2$ nanostructure [33].

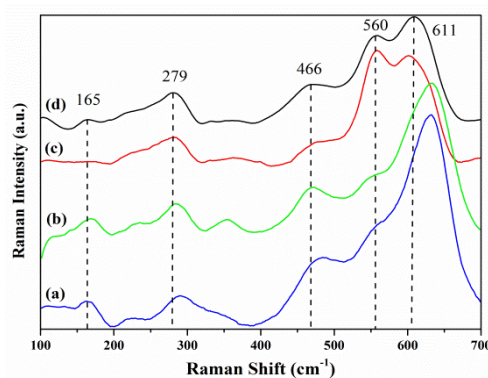


Fig. 8. Raman Spectra for porous NaMnCoO_2 polymeric intermediate (a) before calcination; (b) 400°C; (c) 600°C; (d) 800°C.

The wide Raman peaks indicates that the particles for layered P3-type $\text{Na}_{0.67}\text{Mn}_{0.3}\text{Co}_{0.7}\text{O}_2$ are in the nanoscale range [34]. The Raman peaks indicated to formation of layered sodium – metal transition oxides structure in all four samples and this structure developed and defined with increasing the calcination temperatures, and well agreed with SEM, XRD and TGA results.

Table 3. Raman peaks numbers for porous NaMnCoO_2 polymeric intermediate before calcination and calcined at 400, 600 and 800°C.

Samples	Peak 1 cm^{-1}	Peak 2 cm^{-1}	Peak 3 cm^{-1}	Peak 4 cm^{-1}	Peak 5 cm^{-1}
Polymeric intermediate	166	290	481	556	632
400 °C	170	285	470	556	631
600 °C	165	283	471	559	601
800 °C	165	279	466	560	611

3.7. Electrochemical measurements

3.7.1. Galvanostatic charge/discharge

After studying the effect of calcination temperature on the morphological and structural properties of P-type NaMnCoO₂ cathodes, the influence on the electrochemical performance was also investigated. Galvanostatic charge/discharge performance for layered NaMnCoO₂ cathodes with different calcinations temperatures (400, 600, 800°C) was carried out using Multichannel Potentiostat/GalvanostatOrigaflex- OGF500 work station, two electrode cells with constant current densities at different scan rates (1 C, 0.5 C, 0.25 C) and specific voltage windows were applied to characterize the assembled batteries charge/discharge capacities at room temperature (25°C). Figure.9 (a, b, c) shows the charge/discharge capacity profiles as a function of charge/discharge specific capacity for three NaMnCoO₂ cathodes calcined at 400, 600 and 800°C respectively, with different current densities (1 C, 0.5 C, 0.25 C) to estimate the rate capability of prepared electrodes. The charge/discharge capacity can be computed by the total applied current multiply with exposure time. The batteries were assembled using sodium metal as counter and reference electrodes cycled in specific voltage windows. The obtained charge/discharge curves for prepared batteries were recorded after several cycles with low current densities in order to activate and stabilize the batteries components and keep them in full contact after assembling to gain the best electrochemical performance [35]. From the obtained voltage profiles of cathodes calcined at (400, 600, 800°C), the cathode calcined at 400°C shows smooth and symmetric charge/discharge curves at all the current densities (1, 0.5, 0.25 C) with voltage windows (3.5-1.5 V), (3.1- 2.2 V), (2.9- 2.5 V) vs. Na⁺/Na respectively, the faradic reactions of this cathode are reversible which means that during the charging and discharging process there is the same amount of sodium ions extracted and intercalated back into layered cathode structure at specific closed circuit voltage leading to good mobility for Na ions during layered structure [36, 37], while the cathodes calcined at 600 and 800°C shows also smooth and symmetric charge/discharge curves with voltage windows (5-1.9 V) and (4.5-1.6 V) at 1 C, (3.4-2.2 V) and (3.7-2 V) at 0.5 C and (3.1-2.4 V) and (3.3-2.3 V) at 0.25 C vs. Na⁺/Na, excepting at scan rate (1 C) and (1 and 0.5 C) were smooth and asymmetric curves for 600 and 800°C respectively, exhibiting broad plateaus accompanying with charging curves as shown in Figure.9 (b, c), which are attributable to structural transformations in the cathode crystalline lattice when the sodium ions are extracted from the cathode structure at high voltage operation [38, 39], The charge/discharge curves of prepared layered NaMnCoO₂ cathodes revealed specific capacity and voltage window for each current density (1C, 0.5C, 0.25C). The cathodes calcined at 800 and 600°C yielded the highest output charge/discharge capacities, the discharge capacities at different current densities were 134.7 (1C), 148.2 (0.5C) and 158.3 (0.25C) mAh/g, and 89.3 (1C), 111.6 (0.5C) and 123.4 (0.25C) mAh/g respectively, comparing with the discharge capacity for cathode calcined at 400°C at different current densities 33.9 (1C), 37.7 (0.5C) and 40.9 (0.25C) mAh/g, capacities values progressively decrease with increasing the current density due to the high rate switches the stored chemical energy inside the battery (discharging) or outer electrical energy (charging) to irreversible chemical processes leads to reduced capacitance values, agreeing with literatures [8, 40, 41].

The results demonstrated that raising the calcination temperatures led to increased capacitance values about three times for calcined cathode at 600°C and four times for 800°C comparing with the calcined cathode at 400°C, these results are completely compatible with the fact that the capacity increases with development of crystal structure and crystallization degree of cathode material as a function of calcination temperature, which is an effective way to improve the electrochemical features [42], Therefore, the cathode calcined at 800°C has the best crystallization degree as discussed in XRD and SEM results, recorded the highest capacitance value 158.3 mAh/g at 0.25C by formation almost the ideal structure for P3-type Na_{0.67}Mn_{0.3}Co_{0.7}O₂ after many structural transformations which corresponds with SEM and TGA results, in other words, the different calcination temperatures lead to different structural properties for the same sample. The calcination temperature clearly affects the electrochemical performance; the increase of calcination temperature reinforced the capacity as shown in Fig. 9, attributed to the orthorhombic ordering, as a result of Na_{0.67}Mn_{0.3}Co_{0.7}O₂ nanocrystal growth by driving the propagation mechanism over the grain boundaries [43].

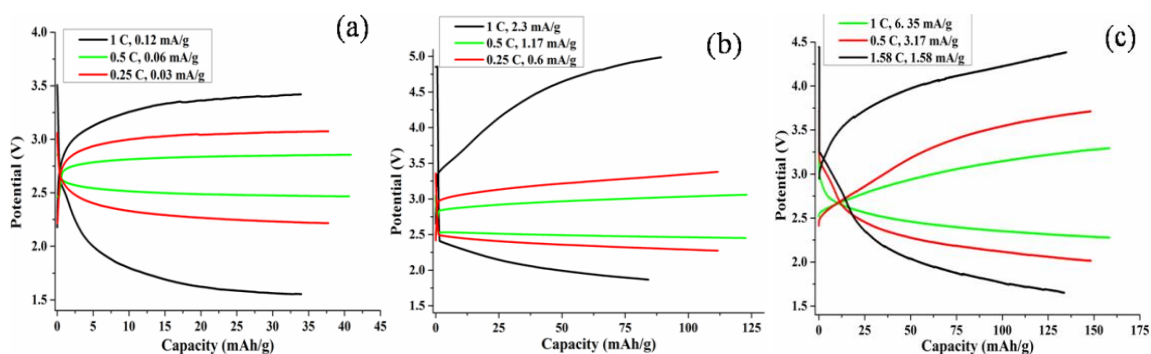


Fig. 9. Charge-discharge specific capacity for calcined NaMnCoO_2 cathodes at (a) 400°C ; (b) 600°C ; (c) 800°C at different current density 1 C, 0.5 C, 0.25 C.

The P3-type structure is considered the most attractive structure as well as P2-type from electrochemical standpoint, where the Na ions insertion proceeds at voltage upper than 3.5 V vs. Na^+/Na [44], while it was obvious that the cathode calcined at 400°C registered the lowest charge/discharge capacity 40.9 mAh/g at 0.25C which is consistent with imperfect formation of $\text{NaMn}_{0.82}\text{Co}_{0.82}\text{O}_2$ structure as revealed by XRD results.

The rate capability test was performed for all prepared cathodes (400 , 600 , 800°C) to verify the effect of calcination temperature on cathodes rate capability, by charge/discharge the assembled batteries at different current densities (1, 0.5, 0.25C) with three cycles for each current density as shown in Figure.10, the cathode calcined at 800°C recorded the highest charge/discharge capacity value at all current densities after three cycles comparing with other cathodes, the discharge capacities for this cathode were 158.3, 148.2 and 134.7 mAh/g at current density 0.25 C, 0.5 C and 1 C respectively, the discharge capacity for this cathode after three cycles became 157.8 mAh/g which indicated to distinguished capacity retention about (99.6%) of the initial capacity and develop the capacity retention for sodium battery, generally all the cathodes shown good cycling stability after three cycles at (0.25 C), the improvement in rate capability and cycling stability attributed to settled intercalation/deintercalation of sodium ions through the cathode structure during cycling process [45, 46].

From another side, the rate capability profile demonstrated that the charging capacities were a bit higher than discharging capacities and these capacities values insignificant decreased after cell cycling, this refers to sluggish kinetics during cathode phase transition and sodium ions intercalation in cathode structure during discharging process as well as possible deintercalation structural sodium ions from the host cathode framework during charging process, which always controls the drooping of capacitance and rate capability [47, 48].

The results demonstrated an improvement in capacity and structural stability for P3-type layered $\text{Na}_{0.67}\text{Mn}_{0.3}\text{Co}_{0.7}\text{O}_2$ cathode calcined 800°C with discharge capacity 158.3 mAh/g, these results are motivated by comparing with previous literatures as $\text{Na}_{0.66}\text{Mn}_{0.5}\text{Co}_{0.5}\text{O}_2$ cathode prepared by X. Wang et al. using one-step solid-state reaction achieved discharge capacity 123 mAh/g [9], and D. Zhou al. et., prepared $\text{Na}_{0.67}\text{Co}_{0.67}\text{Mn}_{0.33}\text{O}_2$ cathode using conventional solid-state reaction delivered discharge capacity 84.7 mAh/g[49].

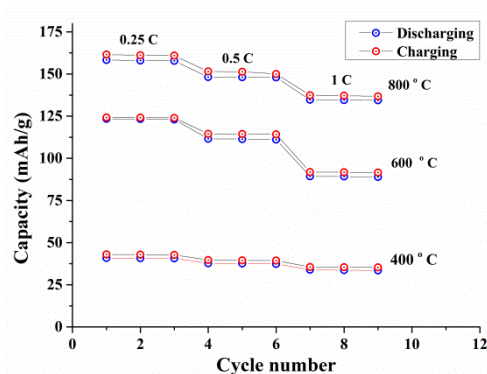


Fig. 10. Charge/discharge capacity for calcined layered NaMnCoO₂ cathodes at 400, 600 and 800 °C with various C-rates (1C, 0.5C, 0.25C) as a function of cycle number.

3.8. Electrochemical impedance spectroscopy (EIS)

Electrochemical impedance spectroscopy (EIS) was carried out for all prepared cathodes to investigate the effect of different calcination temperatures on the rate capability and cyclability of layered P3-type NaMnCoO₂ cathode batteries and to understand the connection between the electrochemical performance and crystal structure. EIS test was performed using electrochemical workstation Multichannel Potentiostat/GalvanostatOrigaflex- OGF500 at room temperature (25 °C) with amplitude 10 mV from high to low frequency (1 mHz - 100 KHz) in automatic sweep mode. EIS spectra were recorded after several charging/discharging cycles to activate the batteries components, the batteries left for 5 hours to return for equilibrium state.

Figure.11 (a, b) represents Nyquist plots for NaMnCoO₂ cathodes calcined at different temperatures (400, 600, 800 °C), the obtained results show clear and significant difference between EIS spectra for cathodes; this is evidence of obvious change in the electronic resistivity of electrodes structure as a function of calcination temperatures. All Nyquist plots for cathodes exhibited two semicircles with different radius and sloping line, the first semicircle in high frequency area was attributed to surface electrolyte inter phase film (SEI) resistance (R_f), the second semicircle and sloping line in medium and low frequency area was attributed to charge transfer resistance (R_{ct}) [50, 51].

The cathode calcined at 400 °C offered small-radius semicircle in high frequency area and big-radius semicircle and sloping line in low and medium frequency areas, the cathodes calcined at 600 °C offered big-radius semicircle in high frequency area and very small-radius semicircle and sloping line in medium and low frequency areas while the cathode calcined at 800 °C offered two semicircles with very small-radius in all frequency areas, these results revealed that charge transfer resistance (R_{ct}) of electrodes obviously decreased as a function of increasing calcination temperature. The cathode at 400 °C has the highest charge transfer resistance (high electronic resistance) which was attributed to uncompleted phase crystallization at this temperature, comparing with cathodes at 600 and 800 °C that recorded highest charge conductivity respectively, depending on semicircles-radius in medium and low frequency areas indicated high crystallization degree at these temperatures due to easier Na ions transfer during the sodiation/desodiation reactions [38, 50, 52], corresponding with SEM, XRD and TGA results. EIS test was carried out to confirm that the layered P3-type Na_{0.67}Mn_{0.3}Co_{0.7}O₂ calcined at 800 °C has good rate capability and cyclability than cathodes calcined at 400 and 600 °C.

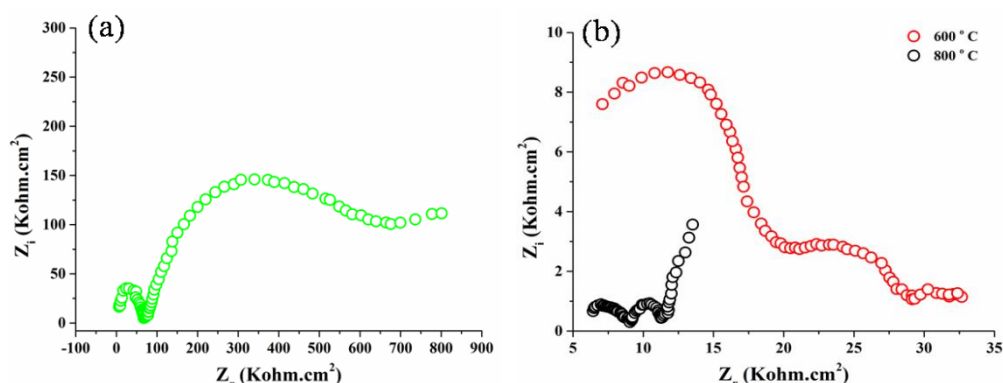


Fig. 11. Nyquist plots for NaMnCoO₂ cathodes calcined at (a) 400°C; (b) 600°C; and 800°C vs Na⁺/Na.

4. Conclusions

In summary, layered P3-type NaMnCoO₂ nanostructures were prepared the first time by novel low cost citric-urea self-combustion route as cathode materials for Na ion battery, the effect of different calcination temperatures on the crystallization degree and electrochemical performance were investigated. The results demonstrated that increasing the calcination temperature leads to improved crystalline growth degree and electronic ordering of cathodes powders, the capacity increased as a function of calcination temperature. The layered P3-type Na_{0.67}Mn_{0.3}Co_{0.7}O₂ powder calcined at 800°C revealed the best structural and electrochemical performance with delivered discharge capacity (158.3 mAh/g) as appropriate cathode material for Na ion battery at current density (0.25 C), and good cyclability, rate capability with capacity retention about (99.6 %) were achieved. Therefore, stable layered P3-type Na_{0.67}Mn_{0.3}Co_{0.7}O₂ is an effective alternative cathode material for Na ion battery in term of distinctive electrochemical performance.

Acknowledgments

This work was supported by a grant of the Romanian Ministry of Research and Innovation, PCCDI-UEFISCDI, project number PN-III-P1-1.2-PCCDI-2017-0185/2018 (76PCCDI/2018), within PNCDI III.

References

- [1] A. F. Hollemann, E. Wiberg, N. Wiberg, Lehrbuch der Anorganischen Chemie, 91.-100. Auflage. Walter de Gruyter, Berlin, **999**, 1012 (1985).
- [2] J. M. Tarascon, Nature chemistry **2**(6), 510 (2010).
- [3] V. Palomares, P. Serras, I. Villaluenga, K. B. Hueso, J. Carretero-González, T. Rojo, Energy & Environmental Science **5**(3), 5884 (2012).
- [4] J. Molenda, C. Delmas, P. Hagenmuller, Solid State Ionics **9**, 431 (1983).
- [5] K. West, B. Zachau-Christiansen, T. Jacobsen, S. Skaarup, Solid State Ionics **28**, 1128 (1988).
- [6] H. Yoshida, N. Yabuuchi, K. Kubota, I. Ikeuchi, A. Garsuch, M. Schulz-Dobrick, S. Komaba, Chemical communications **50**(28), 3677 (2014).

- [7] E. Lee, J. Lu, Y. Ren, X. Luo, X. Zhang, J. Wen, D. Kim, *Advanced Energy Materials* **4**(17), 1400458 (2014).
- [8] M. Sathiya, K. Hemalatha, K. Ramesha, J. M. Tarascon, A. S. Prakash, *Chemistry of Materials* **24**(10), 1846 (2012).
- [9] X. Wang, M. Tamaru, M. Okubo, A. Yamada, *The Journal of Physical Chemistry C* **117**(30), 15545 (2013).
- [10] A. S. Mukasyan, P. Dinka, *International Journal of Self-Propagating High-Temperature Synthesis* **16**(1), 23 (2007).
- [11] A. Sutka, G. Mezinskis, *Frontiers of Materials Science* **6**(2), 128 (2012).
- [12] C. C. Hwang, J. S. Tsai, T. H. Huang, C. H. Peng, S. Y. Chen, *Journal of Solid State Chemistry* **178**(1), 382 (2005).
- [13] *International Tables for Crystallography Vol. A, Space group* **141**, pp. 482 (2006).
- [14] F. Hulliger, *Structural chemistry of layer-type phases, Springer Science & Business Media, discussion for special compounds* **5**, 49 (2012).
- [15] J. M. Paulsen, J. R. Dahn, *Solid State Ionics* **126**(1-2), 3 (1999).
- [16] N. A. Nguyen, K. Kim, K. H. Choi, H. Jeon, K. Lee, M. H. Ryou, Y. M. Lee, *Journal of The Electrochemical Society* **164**(1), A6308 (2017).
- [17] W. D. Kingery, H. K. Bowen, D. R. Uhlmann, *Introduction to ceramics Vol. 183*, New York: Wiley, 1976.
- [18] S. H. Park, S. H. Kang, I. Belharouak, Y. K. Sun, K. Amine, *Journal of Power Sources* **177**(1), 177 (2008).
- [19] I. Hasa, D. Buchholz, S. Passerini, B. Scrosati, J. Hassoun, *Advanced Energy Materials* **4**(15), 1400083 (2014).
- [20] S. Vivekanandhan, M. Venkateswarlu, N. Satyanarayana, *Advanced Device Materials* **1**(4), 100 (2015).
- [21] W. Liu, G. C. Farrington, F. Chaput, B. Dunn, *Journal of the Electrochemical Society* **143**(3), 879 (1996).
- [22] W. L. Guo, L. Q. Mai, W. Chen, Q. Xu, Q. Y. Zhu, *Journal of Materials Science Letters* **22**(14), 1035 (2003).
- [23] S. Hildebrandt, A. Eva, P. Komissinskiy, C. Fasel, I. Fritsch, L. Alff, *Journal of sol-gel science and technology* **63**(3), 307 (2012).
- [24] C. Julien, C. Letranchant, S. Rangan, M. Lemal, S. Ziolkiewicz, S. Castro-Garcia, M. Benkaddour, *Materials Science and Engineering: B* **76**(2), 145 (2000).
- [25] W. Huang, R. Frech, *Solid State Ionics* **86**, 395 (1996).
- [26] K. M. Shaju, K. V. Ramanujachary, S. E. Lofland, G. S. Rao, B. V. R. Chowdari, *Journal of Materials Chemistry* **13**(10), 2633 (2003).
- [27] D. Berger, N. van Landschoat, C. Ionica, F. Papa, V. Fruth, *J. Optoelectron. Adv. M.* **5**, 719 (2003).
- [28] T. J. Richardson, S. J. Wen, K. A. Strichel, P. N. Ross Jr, E. J. Cairns, *Materials research bulletin* **32**(5), 609 (1997).
- [29] K. Singh, B. Kirubasankar, S. Angaiah, *Ionics* **23**(3), 731 (2017).
- [30] J. Tang, Y. Wang, L. Wang, J. Zhao, Y. Li, *Materials Chemistry and Physics* **224**, 1 (2019).
- [31] Y. Wang, J. Tang, X. Yang, W. Huang, *Inorganic Chemistry Frontiers* **5**(3), 577 (2018).
- [32] G. Singh, J. M. L. del Amo, M. Galceran, S. Pérez-Villar, T. Rojo, *Journal of Materials Chemistry A* **3**(13), 6954 (2015).
- [33] T. Gao, M. Glerup, F. Krumeich, R. Nesper, H. Fjellvåg, P. Norby, *The Journal of Physical Chemistry C* **112**(34), 13134 (2008).
- [34] Y. G. Shi, Y. L. Liu, H. X. Yang, C. J. Nie, R. Jin, J. Q. Li, *Physical Review B* **70**(5), 052502 (2004).
- [35] H. V. Ramasamy, K. Kaliyappan, R. Thangavel, W. M. Seong, K. Kang, Z. Chen, Y. S. Lee, *The journal of physical chemistry letters* **8**(20), 5021 (2017).

- [36] L. Athouël, F. Moser, R. Dugas, O. Crosnier, D. Bélanger, T. Brousse, *The Journal of Physical Chemistry C* **112**(18), 7270 (2008).
- [37] A. Caballero, L. Hernan, J. Morales, L. Sanchez, J. Santos, *Journal of Solid-State Chemistry* **174**(2), 365 (2003).
- [38] K. Kaliyappan, J. Liu, B. Xiao, A. Lushington, R. Li, T. K. Sham, X. Sun, *Advanced Functional Materials* **27**(37), 1701870 (2017).
- [39] W. K. Pang, S. Kalluri, V. K. Peterson, N. Sharma, J. Kimpton, B. Johannessen, Z. Guo, *Chemistry of Materials* **27**(8), 3150 (2015).
- [40] D. Buchholz, A. Moretti, R. Kloepsch, S. Nowak, V. Siozios, M. Winter, S. Passerini, *Chemistry of Materials* **25**(2), 142 (2013).
- [41] X. Xu, S. Ji, R. Gao, J. Liu, *RSC Advances* **5**(63), 51454 (2015).
- [42] X. Zhi, G. Liang, L. Wang, X. Ou, J. Zhang, J. Cui, *Journal of Power Sources* **189**(1), 779 (2009).
- [43] F. Huang, H. Zhang, J. F. Banfield, *Nano letters* **3**(3), 373 (2003).
- [44] M. H. Han, E. Gonzalo, S. Singh, T. Rojo, *Energy & Environmental Science* **8**(1), 81 (2015).
- [45] Y. Yin, Y. Hu, P. Wu, H. Zhang, C. Cai, *Chemical Communications* **48**(15), 2137 (2012).
- [46] Y. Fang, L. Xiao, J. Qian, X. Ai, H. Yang, Y. Cao, *Nano letters* **14**(6), 3539 (2014).
- [47] J. Peters, D. Buchholz, S. Passerini, M. Weil, *Energy & Environmental Science* **9**(5), 1744 (2016).
- [48] M. S. Islam, C. A. Fisher, *Chemical Society Reviews* **43**(1), 185 (2014).
- [49] D. Zhou, W. Huang, X. Kang, F. Zhao, L. Zhao, Z. Deng, M. Xiang, *International Journal Of Electrochemical Science* **13**(2), 2010 (2018).
- [50] S. S. Zhang, K. Xu, T. R. Jow, *Electrochimica acta* **49**(7), 1057 (2004).
- [51] Y. K. Sun, J. M. Han, S. T. Myung, S. W. Lee, K. Amine, *Electrochemistry communications* **8**(5), 821 (2006).
- [52] J. Li, C. Daniel, D. Wood, *Journal of Power Sources* **196**(5), 2452 (2011).